

# The non-thermal superbubble in IC 10: the generation of cosmic ray electrons caught in the act

Volker Heesen,<sup>1\*</sup> Elias Brinks,<sup>2</sup> Martin G. H. Krause,<sup>3,4</sup> Jeremy J. Harwood,<sup>2,†</sup> Urvashi Rau,<sup>5</sup> Michael P. Rupen,<sup>5</sup> Deidre A. Hunter,<sup>6</sup> Krzysztof T. Chyży<sup>7</sup> and Ged Kitchener<sup>2</sup>

<sup>1</sup>*School of Physics and Astronomy, University of Southampton, Southampton SO17 1BJ, UK*

<sup>2</sup>*Centre for Astrophysics Research, University of Hertfordshire, Hatfield AL10 9AB, UK*

<sup>3</sup>*Excellence Cluster Universe, Technische Universität München, Boltzmannstrasse 2, D-85748 Garching, Germany*

<sup>4</sup>*Max-Planck-Institut für extraterrestrische Physik, Giessenbachstr. 1, D-85741 Garching, Germany*

<sup>5</sup>*NRAO, P.V.D. Science Operations Center, National Radio Astronomy Observatory, 1003 Lopezville Road, Socorro, NM 87801, USA*

<sup>6</sup>*Lowell Observatory, 1400 West Mars Hill Road, Flagstaff, AZ 86001, USA*

<sup>7</sup>*Obserwatorium Astronomiczne Uniwersytetu Jagiellońskiego, ul. Orła 171, 30-244 Kraków, Poland*

Accepted 2014 October 15. Received 2014 October 15; in original form 2014 September 22

## ABSTRACT

Superbubbles are crucial for stellar feedback, with supposedly high (of the order of 10 per cent) thermalization rates. We combined multiband radio continuum observations from the Very Large Array (VLA) with Effelsberg data to study the non-thermal superbubble (NSB) in IC 10, a starburst dwarf irregular galaxy in the Local Group. Thermal emission was subtracted using a combination of Balmer H $\alpha$  and VLA 32 GHz continuum maps. The bubble’s non-thermal spectrum between 1.5 and 8.8 GHz displays curvature and can be well fitted with a standard model of an ageing cosmic ray electron population. With a derived equipartition magnetic field strength of  $44 \pm 8 \mu\text{G}$ , and measuring the radiation energy density from *Spitzer* MIPS maps as  $5 \pm 1 \times 10^{-11} \text{ erg cm}^{-3}$ , we determine, based on the spectral curvature, a spectral age of the bubble of  $1.0 \pm 0.3 \text{ Myr}$ . Analysis of the LITTLE THINGS H I data cube shows an expanding H I hole with 100 pc diameter and a dynamical age of  $3.8 \pm 0.3 \text{ Myr}$ , centred to within 16 pc on IC 10 X-1, a massive stellar mass black hole ( $M > 23 M_{\odot}$ ). The results are consistent with the expected evolution for a superbubble with a few massive stars, where a very energetic event like a Type Ic supernova/hypernova has taken place about 1 Myr ago. We discuss alternatives to this interpretation.

**Key words:** radiation mechanisms: non-thermal – cosmic rays – galaxies: individual: IC 10 – galaxies: irregular – galaxies: starburst – radio continuum: galaxies.

## 1 INTRODUCTION

Stellar feedback is a fundamental process that regulates the formation and evolution of galaxies. Supernovae (SNe) inject energy into the interstellar medium (ISM), heating the gas to X-ray emitting temperatures and accelerating cosmic rays via shock waves. Galactic winds, hybridly driven by the hot gas and cosmic rays, remove mass and angular momentum (Everett et al. 2008; Strickland & Heckman 2009; Dorfi & Breitschwerdt 2012; Hanasz et al. 2013; Salem & Bryan 2014). Cosmological simulations without stellar feedback not only predict wrong global mass estimates, but mass concentrations towards the centres of galaxies

that are too high, leading to rotation curves that are steeper than observed (Scannapieco 2013). The most abundant type of galaxies in the local Universe, dwarf galaxies, are particularly affected by outflows: their weak gravitational potentials make them susceptible to outflows and winds (Tremonti et al. 2004). In the paradigm of a  $\Lambda$ CDM Universe, the removal of baryons in the least massive dark matter haloes may resolve the long standing ‘missing satellites’ problem (Moore et al. 1999). The loss of baryonic matter and associated angular momentum at early stages in their formation and evolution can affect the distribution of the non-baryonic matter as well, rendering the inner part of the rotation curves less steep (Governato et al. 2010; Oh et al. 2011a,b). Furthermore, outflows and winds in dwarf galaxies may be behind the magnetization of the early Universe (e.g. Pakmor, Marinacci & Springel 2014; Siejkowski et al. 2014).

\* E-mail: v.heesen@soton.ac.uk

† Now at ASTRON, Postbus 2, 7990 AA Dwingeloo, the Netherlands.

Massive stars are the agents of stellar feedback and they manifest themselves by carving bubbles – cavities of tenuous, hot gas – into the ISM. They usually form in groups, so that their bubbles start to overlap when expanding and subsequently merge, forming larger structures in excess of 100 pc, so-called superbubbles. The wind of massive stars, especially during their Wolf–Rayet (WR) phase, powers the early expansion of the bubble. Subsequent SNe create strong shocks in the bubble interior that are responsible for the thermal X-ray and the non-thermal synchrotron emitting gas (Krause et al. 2014). Stellar feedback in the form of SNe is more efficient for clustered SNe than for randomly distributed ones as subsequent SNe explode in the tenuous gas of the bubble and their shock waves are not suffering from strong radiative cooling. Hence, the thermalization fraction of clustered SNe is higher (Krause et al. 2013).

An intriguing example of SN feedback is presented by what has become known as the non-thermal superbubble (NSB; Yang & Skillman 1993) in the nearby dwarf irregular galaxy IC 10, a member of the Local Group at a distance of 0.7 Mpc (1 arcsec = 3.4 pc; Hunter et al. 2012). It has several young star clusters, containing massive stars (Hunter 2001) and an unusually high number of WR stars (Massey & Holmes 2002). IC 10 is a dwarf irregular galaxy that is currently undergoing a starburst phase. Close to the centre of the NSB is one of the heaviest stellar-mass black holes known at a remnant mass of  $>23 M_{\odot}$  (Silverman & Filippenko 2008), which forms together with the massive WR star [MAC92] 17A a highly variable luminous X-ray binary, known as IC 10 X-1 (J2000.0, RA 00<sup>h</sup>20<sup>m</sup>29<sup>s</sup>.09, Dec. 59°16′51″.95; Bauer & Brandt 2004; Barnard et al. 2014). It has been speculated that a core collapse of the IC 10 X-1 progenitor in a ‘hypernova’ could be responsible for the NSB, rather than a series of SNe (Lozinskaya & Moiseev 2007).

In this Letter, we present multiband radio continuum observations with the NRAO<sup>1</sup> Karl G. Jansky Very Large Array (VLA) to study the non-thermal radio continuum spectrum of the NSB. This project follows on, and extends some preliminary results presented in Heesen et al. (2011). The data cover the frequency range between 1.4 and 32 GHz, at high spatial resolution.

## 2 OBSERVATIONS

We observed IC 10 with the VLA (project ID: AH1006). Observations were taken in D-array in 2010 August and September at *L* band (1.4–1.6 GHz), *C* band (4.5–5.4 and 6.9–7.8 GHz), *X* band (7.9–8.8 GHz) and *Ka* band (27–28 and 37–38 GHz) with  $\approx 3$  h on-source time each. In addition, we observed in C-array at *L*, *C* and *X* band with  $\approx 3$  h on-source time each in 2012 February to April (ID: 12A-288) and 2013 August (ID: 13A-328). A flux calibrator (3C 48) was observed either at the beginning or the end of the observations, and scans of IC 10 were interleaved every 15 min with a 2 min scan of a nearby complex gain calibrator (J0102+5824). We incorporated *L*-band B-array data observed with the historical VLA in 1986 September (ID: AS0266) from Yang & Skillman (1993).

We followed standard data reduction procedures, using the Common Astronomy Software Applications package (CASA), developed by NRAO, and utilizing the flux scale by Perley & Butler (2013). We self-calibrated the *L*-, *C*- and *X*-band data with two

rounds of phase-only antenna-based gain corrections, using images from the C-array data as a model. In *C* and *X* bands, we self-calibrated in phase and amplitude, adding in the D-array data (self-calibrated in phase), checking that the amplitudes did not change by more than 1–2 per cent. For the imaging we used CASA’s implementation of the Multi-Scale Multi-Frequency Synthesis (MS–MFS) algorithm (Rau & Cornwell 2011), which simultaneously solves for spatial and spectral structure during wide-band image reconstruction. A radio spectral index image was produced by MS–MFS as well, which we used to refine the self-calibration model. A post-deconvolution wide-band primary beam correction was applied to remove the effect of the frequency-dependent primary beam. For the spectral analysis, we imaged subsets (‘spectral windows’) of data with either 128 or 256 MHz bandwidth, varying Briggs’ ‘robust’ parameter as function of frequency to achieve a synthesized beam of a similar angular size. All data were convolved with a Gaussian kernel in AIPS<sup>2</sup> to an identical resolution of 5.1 arcsec and regridded.

Because the VLA cannot record baselines smaller than  $\approx 30$  m (elevation dependent), there is a limit to the largest angular scale that can be observed, resulting broadly in flux densities that are too low compared with single-dish measurements; this is known as the ‘missing zero-spacing flux’. Our VLA flux density at 1.5 GHz and those at 2.6 and 10.5 GHz, measured with the 100-m Effelsberg telescope (Chyży et al. 2003, 2011), of 343, 277 and 156 mJy, can be fitted with a constant spectral index of  $-0.41$ . We can interpolate them to estimate the missing zero-spacing flux in each spectral window. We found that at frequencies of 4–6 GHz, 10–20 per cent of the flux density was missed by the VLA, which increased to 30–40 per cent at frequencies of 7–9 GHz. In order to correct for this, we merged the VLA and Effelsberg data using IMERG in AIPS. We used the VLA 1.5 GHz map as a template for the large-scale emission at the lower end of our frequency range, which has the benefit of an improved angular resolution in comparison to the 2.6 GHz Effelsberg map. We hence interpolated the 1.5 GHz VLA and 10.5 GHz Effelsberg maps at an angular resolution of 78 arcsec, assuming a constant but spatially resolved spectral index, to have a template of the large-scale emission in each spectral window. We merged the data of each spectral window with the appropriate template, making sure that the integrated flux densities of several regions agreed to within 5–10 per cent and the discrepancy between the total integrated flux densities was less than 4 per cent. This was achieved by adjusting the ‘uvrange’ parameter in IMERG, which prescribes the angular scale at which the single-dish image is scaled to interferometric image; we used values within the range of 0.8–1.8 k $\lambda$ .

## 3 RESULTS

In Fig. 1(a), we present a 6.2 GHz contour map from combined VLA and Effelsberg observations at 3.4 arcsec angular resolution, overlaid on an integrated H I map from LITTLE THINGS (Hunter et al. 2012). The NSB is centred on RA 00<sup>h</sup>20<sup>m</sup>28<sup>s</sup>.85, Dec. 59°16′48″, which is 5 arcsec south-west of IC 10 X-1, and has a diameter of 54 arcsec or 184 pc. We created a map of the thermal (free–free) emission from the Balmer H $\alpha$  emission map of Hunter & Elmegreen (2004) following standard conversion (e.g., Deeg, Duric & Brinks 1997, equation 3,  $T = 10^4$  K),

<sup>1</sup> The National Radio Astronomy Observatory is a facility of the National Science Foundation operated under cooperative agreement by Associated Universities, Inc.

<sup>2</sup> AIPS, the Astronomical Image Processing Software, is free software available from the NRAO.

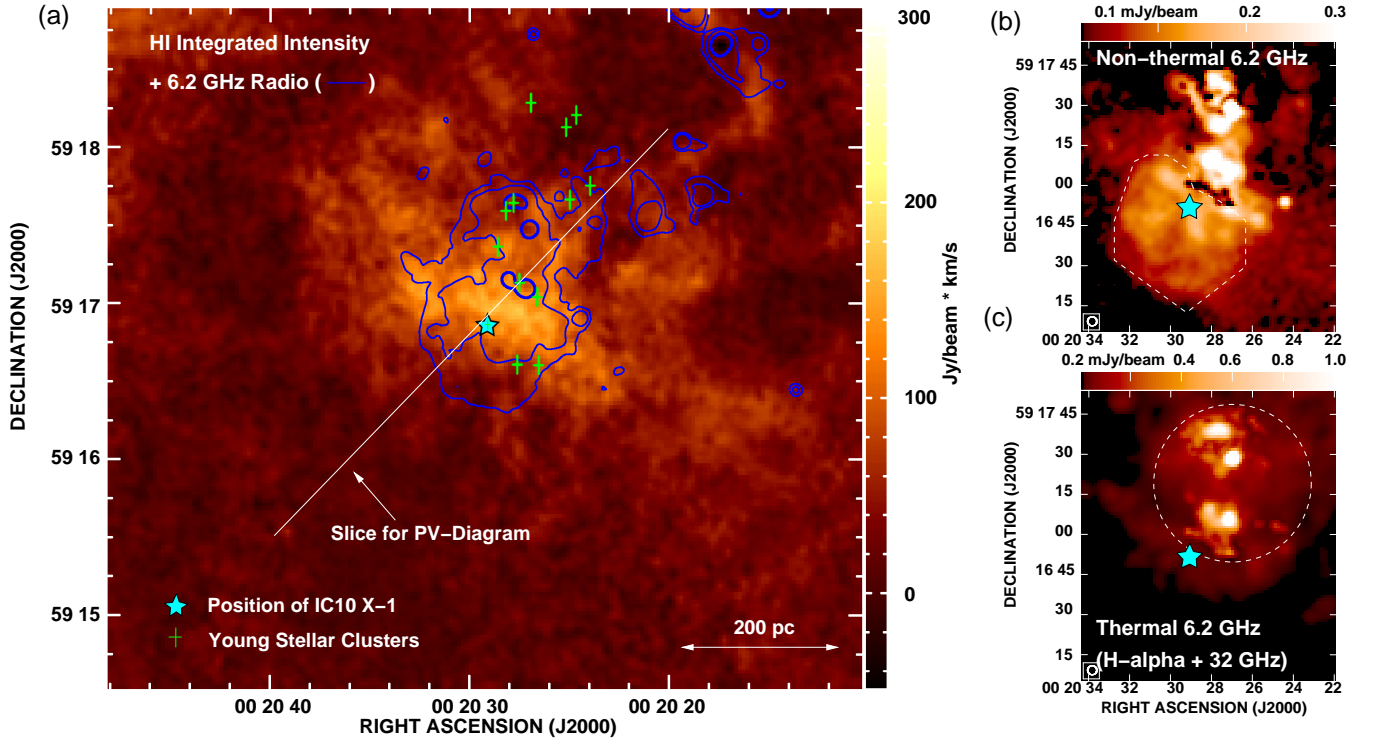


**Figure 1.** (a) Integrated HI emission line intensity as grey-scale at  $5.5 \times 5.9$  arcsec (PA =  $16^\circ$ ) resolution of an approximately  $1 \text{ kpc}^2$  region to the south-east of the centre of IC 10. Contours show the 6.2 GHz radio continuum emission at 60, 120 and  $800 \mu\text{Jy beam}^{-1}$ , i.e. the superposition of thermal and non-thermal emission. The white line corresponds to the slice used to extract the *PV*-diagram at an angle of  $-45^\circ$ , centred on the HI hole (see the text for details). Green plus signs show the position of stellar clusters (Hunter 2001). (b) Non-thermal radio continuum at 6.2 GHz of the superbubble, where the dashed line indicates the region, used for measuring the spectrum of the non-thermal superbubble. (c) Thermal radio continuum of the same region as in (b), constructed from a combination of H $\alpha$  and 32 GHz emission. The dashed line indicates the 80 per cent attenuation level of the primary beam at 32 GHz. In panels (a)–(c), the magenta star indicates the position of IC 10 X-1 and the angular resolution of the radio data is 3.4 arcsec (equivalent to 12 pc).

where we corrected for foreground absorption using  $E(B - V) = 0.75 \text{ mag}$  (Burstein & Heiles 1984). This map was combined with our 32 GHz map of the south-eastern starburst region, which we use as an extinction free measurement of the thermal radio continuum emission (Fig. 1 c). A comparison between the two maps showed agreement to within 10–20 per cent in areas outside of the compact H II regions ( $I_{\text{th}} < 1.0 \text{ mJy beam}^{-1}$ ), indicating that our estimate of the optical foreground absorption is accurate.

The main fraction of thermal radio continuum is located in the H II regions, north-west of the NSB. Whereas the NSB is prominent in the non-thermal radio continuum, there has thus far been little other evidence reported in the literature that the NSB constitutes a cavity in the ISM. Wilcots & Miller (1998) find an HI hole at its position, but do not report any signs of expansion. There is weak, diffuse H $\alpha$  emission from ionized hydrogen and an increased line width, corresponding to a thermal velocity dispersion of  $35 \text{ km s}^{-1}$ , but nothing to suggest an expanding shell (Thurrow & Wilcots 2005). Using the natural weighted HI data cube from LITTLE THINGS (FWHM =  $8.4 \times 7.5$  arcsec, PA =  $37^\circ$ ; Hunter et al. 2012), we have created a position–velocity diagram of the NSB and its surroundings, presented in Fig. 2. We find a cavity of little prominence, centred on RA  $00^{\text{h}}20^{\text{m}}29^{\text{s}}.71$ , Dec.  $59^\circ16'51''.9$ , which is 4.8 arcsec east of IC 10 X-1. It is either a single HI hole with a diameter of 100 pc and an extent in velocity space of  $30 \text{ km s}^{-1}$ , or consists of two smaller HI holes with diameters of 76 pc and extents in velocity space of  $18 \text{ km s}^{-1}$  each. For a single hole the expansion velocity is  $15 \text{ km s}^{-1}$ , leading to an es-

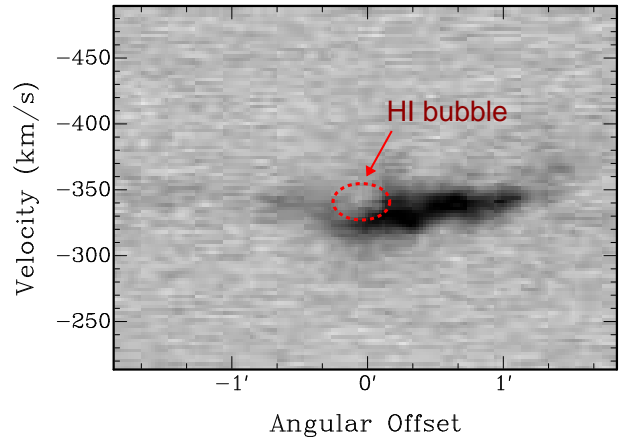


**Figure 2.** Position–velocity (*PV*) diagram of the NSB and its surroundings, from the LITTLE THINGS HI data cube. The position of the slice is shown in Fig. 1(a). South-east is to the left, north-west to the right.

timate of the bubble’s dynamical age of  $\tau_{\text{dyn}} = 3.8 \pm 0.5 \text{ Myr}$ , with a similar age for the double-hole scenario.

For further analysis, we fed the radio continuum data into the Broadband Radio Analysis Tools (BRATS; Harwood et al. 2013). The spectrum of the NSB presented in Fig. 3 (flux densities are tabulated in Table 1) shows a conspicuous curvature, which can be well fitted by a Jaffe–Perola (JP; Jaffe & Perola 1973) model, shown as red solid line, with an injection spectral index of  $\alpha_{\text{inj}} =$

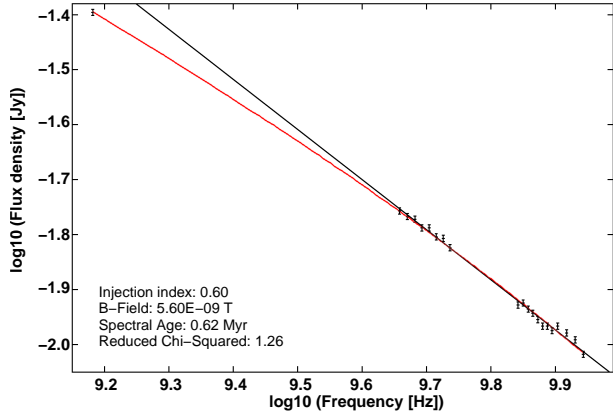


**Figure 3.** Non-thermal spectrum of the NSB between 1.5 and 8.8 GHz. The solid red line shows the Jaffe–Perola model fit to the data and the solid black line is a linear fit to data points  $>1.5$  GHz.

**Table 1.** Non-thermal flux densities of the NSB.

$\nu$ (GHz)	$S_\nu$ (mJy)	$\nu$ (GHz)	$S_\nu$ (mJy)	$\nu$ (GHz)	$S_\nu$ (mJy)
1.52	40.2	5.32	15.6	7.59	10.8
4.55	17.5	5.45	15.0	7.72	10.8
4.68	17.1	6.95	11.8	7.85	10.6
4.81	16.9	7.08	11.9	8.01	10.8
4.93	16.3	7.21	11.6	8.27	10.5
5.06	16.3	7.33	11.4	8.53	10.2
5.19	15.7	7.46	11.1	8.78	9.6

$0.6 \pm 0.1$ . The JP model describes the evolution of radio continuum emission from a cosmic ray electron (CRE) population within a constant magnetic field strength following a single-injection. There exist variations to the JP model, such as the KP (Kardashev 1962) and Tribble (Tribble 1993) model. Our data cannot differentiate between them as any differences are only notable close to the break frequency. Assuming energy equipartition and using the revised equipartition formula by Beck & Krause (2005), we find a total magnetic field strength of  $44 \pm 8 \mu\text{G}$  ( $U_B = 7.7 \pm 0.4 \times 10^{-11} \text{ erg cm}^{-3}$ ). The total infrared luminosity from *Spitzer* MIPS 24–160  $\mu\text{m}$  maps from Dale & Helou (2002) lead to a radiation energy density of  $U_{\text{rad}} = U_{\text{star}} + U_{\text{IR}} = 5 \pm 1 \times 10^{-11} \text{ erg cm}^{-3}$ , where the contribution from stellar light is taken as  $U_{\text{star}} = 1.73 \times U_{\text{IR}}$  as measured in the solar neighbourhood (Draine 2011).

The spatially resolved distribution of the spectral age is shown in Fig. 4, where we applied a S/N-cutoff of 5 in each pixel. There is an east–west gradient, where the age in the eastern part is  $\tau = 1.0$  Myr. The JP model fit to the spatially resolved data is better ( $\langle \chi_{\text{red}}^2 \rangle = 0.6$ ) than for the integrated spectrum ( $\chi_{\text{red}}^2 = 1.3$ ), because a superposition of spectral ages cannot be described by a single JP model. This leads us to conclude that our best estimate of the spectral age is  $\tau_{\text{spec}} = 1.0 \pm 0.3$  Myr. The error is a combination of the magnetic field error and the formal fit error of the JP model.

Finally, in order to exclude a power-law spectrum we conducted a few more tests: first, we fitted a power-law fit to the integrated spectrum and found  $\chi_{\text{red}}^2 = 4.5$ , far inferior to the JP model fit. Secondly, a power-law fit to data points  $>1.5$  GHz predicts a flux density at 1.5 GHz of 19 per cent above to the actual value, about 15 times larger than its error of 1.3 per cent (made up of 1 per cent flux calibration error and the rms map noise) as shown in Fig. 3. Thus, we can exclude a spectrum without curvature.

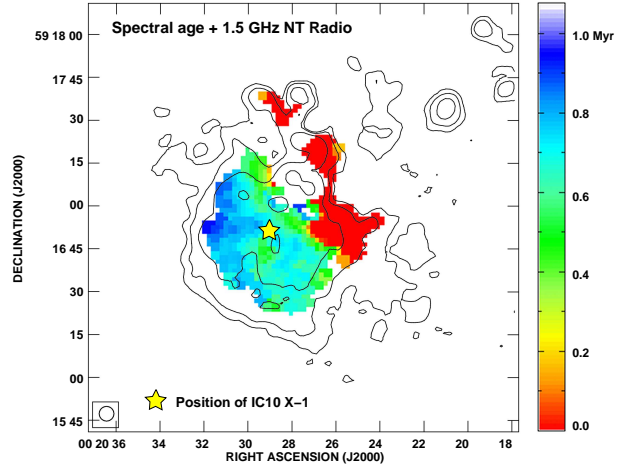


**Figure 4.** Spectral age of the cosmic ray electrons in the NSB and its environment. The angular resolution is 5.1 arcsec (equivalent to 17 pc) as indicated by the boxed circle in the bottom-left corner. Contours show the non-thermal 1.5 GHz emission at  $3, 5, 10, 20$  and  $40 \times 27 \mu\text{Jy beam}^{-1}$  and the yellow star the position of IC 10 X-1.

## 4 DISCUSSION

We first review the parameters derived for the IC 10 NSB: the integrated current cosmic ray energy in the NSB is  $1 \times 10^{51}$  erg, where we modelled the bubble as a sphere and used the assumption of energy equipartition ( $U_{\text{CR}} = U_B$ ), injected approximately 1 Myr ago. Following the calculations of Bagetakos et al. (2011), we can derive the energy required to create the H I hole as  $0.2\text{--}1 \times 10^{51}$  erg, with the upper value appropriate if two holes were formed, where the ambient density of the neutral, atomic gas is  $0.8\text{--}2.2 \text{ cm}^{-3}$  (including helium). The contribution from turbulent gas within the NSB traced in  $\text{H}\alpha$  (Thurrow & Wilcots 2005) is probably not significant when taking into account that the filling factor for emission line gas is probably low.

We can compare our findings with 3D simulations by Krause et al. (2013, 2014). They predict that superbubbles reach diameters of the order of 100 pc even before the first SN. Each SN then first heats the bubble, accelerates the shell, and then dissipates the injected energy entirely at the leading radiative shock wave, and via radiative cooling in mixing regions at the location of the shell, on a time-scale of a few  $10^5$  yr. The shell slows down accordingly, resulting in a discrepancy between spectral and dynamical age. The rather low shell velocity of the IC 10 NSB (high-velocity superbubbles have a few times faster shells, compare e.g. Oey 1996) is indeed expected if the last embedded SN exploded about 1 Myr ago, as suggested by the non-thermal emission. The CRE would have been accelerated as the accompanying shock wave traversed the bubble. Using the method of Bagetakos et al. (2011) on the aforementioned 3D simulations at a similar time, we find  $10^{51}$  erg as minimum energy to create the cavity, in agreement with the upper limit from the observations. The energy found in cosmic rays is however surprisingly large. Assuming an acceleration efficiency of 10 per cent (e.g. Rieger, de Oña-Wilhelmi & Aharonian 2013), at least  $10^{52}$  erg would have to have been released.

Could this have happened in a single explosion? Highly energetic SNe are thought to be related to long duration gamma-ray bursts (e.g. Mazzali et al. 2014, and references therein). The associated Type Ic SNe have energies of up to a few times  $10^{52}$  erg, adequate to account for our observations. We note that a higher

energy than the standard  $10^{51}$  erg would also better explain the high shell velocities in some high-velocity superbubbles (Oey 1996; Krause & Diehl 2014). It is noteworthy that the NSB is centred to within 16 pc on IC 10 X-1, suggesting an association. This system contains at least one massive star, [MAC92] 14A, which has a mass larger than  $17 M_{\odot}$  and more likely  $35 M_{\odot}$  (Silverman & Filippenko 2008), also a possible progenitor for a Type Ic SN. Alternatively, multiple SNe may have exploded in the past 1 Myr. We cannot rule this out from the spectral ageing analysis, because a constant CRe injection rate since approximately 1 Myr would still lead to a spectral downturn, caused by the oldest CRe. However, the position of the stellar clusters (Fig. 1 a) and the distribution of the thermal radio continuum emission and hence that of massive stars (Fig. 1 c), argues against this scenario, because there is no spatial correlation. It is, however, conceivable that a less massive SN has exploded more recently, offset from IC 10 X-1, which could explain the east–west gradient in the spectral age distribution.

Another way to explain the presence of non-thermal particles would be perhaps the energy release from IC 10 X-1. It is a debated possibility that the X-ray emission of black hole binaries partially originates from a jet in addition to that of the more conventional X-ray corona (Grinberg et al. 2014). If the current X-ray luminosity of IC 10 X-1,  $10^{39}$  erg  $s^{-1}$  (Barnard et al. 2014), comes exclusively from the jet, an outburst length of 1 Myr would be sufficient to explain the cosmic ray energy, assuming a 10 per cent acceleration efficiency. One would then have to explain why this channel was so active in the past and by now has ceased almost entirely with no compact radio source observed in the vicinity of IC 10 X-1.

## 5 CONCLUSIONS

In this Letter, we have presented a multiband radio continuum study of the NSB in the nearby starburst dwarf irregular galaxy IC 10. Conventional wisdom tells us that dwarf galaxies are weak in non-thermal (synchrotron) emission, being easily subjected to outflows and winds and not likely able to retain cosmic rays. IC 10 is no exception, it has a large thermal fraction of 50 per cent at 6 GHz and is underluminous in terms of its radio continuum emission compared to its star-formation rate (Heesen et al. 2011, 2014). However, high spatial resolution observations (10–20 pc) show complex cosmic ray and magnetic field distributions. The NSB stands out as the brightest non-thermal structure and its spectrum shows a conspicuous downturn towards higher frequencies, something that to date has rarely been observed in any nearby galaxy.

We fit a JP spectral model to the data, which describes the radio continuum emission of an ageing population of CRe in a constant magnetic field. Estimating the magnetic field from equipartition and the radiation energy density from *Spitzer* MIPS maps, we find a spectral age of  $\tau_{\text{spec}} = 1.0 \pm 0.3$  Myr (uncertainty stems from the errors of the magnetic field and the spectral fitting errors). The bubble’s dynamical age is  $\tau_{\text{dyn}} = 3.8 \pm 0.3$ , measured from the expansion speed of its corresponding ‘HI hole’. Our results suggest that the NSB was generated by the wind of the progenitor of IC 10 X-1, a massive stellar mass black hole, during its main-sequence life and WR phase. Considering alternative explanations, we find that most likely a single energetic explosion of the progenitor of IC 10 X-1 released  $\gtrsim 10^{52}$  erg, accelerating the non-thermal particles and the shell at the same time. The latter than slowed down via interaction with the ambient medium to its current velocity of  $15 \text{ km s}^{-1}$ . We are observing the NSB in the early stages of its

evolution, of what may become over the next few 10–50 Myr a superbubble of a few hundred parsec size visible as a large HI hole.

## ACKNOWLEDGEMENTS

VH acknowledges support from the Science and Technology Facilities Council (STFC) under grant ST/J001600/1. MK acknowledges support by the DFG cluster of excellence ‘Origin and Structure of the Universe’ and by the ISSI project ‘Massive star clusters across the Hubble time’. JJH wishes to thank the University of Hertfordshire for generous financial support and STFC for a STEP award. We thank our referee, Biman Nath, for a constructive and thoughtful report.

## REFERENCES

- Bagetakos I., Brinks E., Walter F., de Blok W. J. G., Usero A., Leroy A. K., Rich J. W., Kennicutt, R. C., Jr. 2011, *AJ*, 141, 23  
 Barnard R., Steiner J. F., Prestwich A. F., Stevens I. R., Clark J. S., Kolb U. C., 2014, *ApJ*, 792, 131  
 Bauer F. E., Brandt W. N., 2004, *ApJ*, 601, L67  
 Beck R., Krause M., 2005, *Astron. Nachr.*, 326, 414  
 Burstein D., Heiles C., 1984, *ApJS*, 54, 33  
 Chyży K. T., Knapik J., Bomans D. J., Klein U., Beck R., Soida M., Urbanik M., 2003, *A&A*, 405, 513  
 Chyży K. T., Weżgowiec M., Beck R., Bomans D. J., 2011, *A&A*, 529, A94  
 Dale D. A., Helou G., 2002, *ApJ*, 576, 159  
 Deeg H.-J., Duric N., Brinks E., 1997, *A&A*, 323, 323  
 Dorfi E. A., Breitschwerdt D., 2012, *A&A*, 540, A77  
 Draine B. T., 2011, *Physics of the Interstellar and Intergalactic Medium*, Princeton University Press, Princeton, NJ  
 Everett J. E., Zweibel E. G., Benjamin R. A., McCammon D., Rocks L., Gallagher, III J. S., 2008, *ApJ*, 674, 258  
 Governato F. et al., 2010, *Nature*, 463, 203  
 Grinberg V. et al., 2014, *A&A*, 565, A1  
 Hanasz M., Lesch H., Naab T., Gawryszczak A., Kowalik K., Wóltański D., 2013, *ApJ*, 777, L38  
 Harwood J. J., Hardcastle M. J., Croston J. H., Goodger J. L., 2013, *MNRAS*, 435, 3353  
 Heesen V., Brinks E., Leroy A. K., Heald G., Braun R., Bigiel F., Beck R., 2014, *AJ*, 147, 103  
 Heesen V., Rau U., Rupen M. P., Brinks E., Hunter D. A., 2011, *ApJ*, 739, L23  
 Hunter D. A., 2001, *ApJ*, 559, 225  
 Hunter D. A., Elmegreen B. G., 2004, *AJ*, 128, 2170  
 Hunter D. A. et al., 2012, *AJ*, 144, 134  
 Jaffe W. J., Perola G. C., 1973, *A&A*, 26, 423  
 Kardashev N. S., 1962, *SvA*, 6, 317  
 Krause M., Diehl R., Böhringer H., Freyberg M., Lubos D., 2014, *A&A*, 566, A94  
 Krause M., Fierlinger K., Diehl R., Burkert A., Voss R., Ziegler U., 2013, *A&A*, 550, A49  
 Krause M. G. H., Diehl R., 2014, *ApJ*, 794, L21  
 Lozinskaya T. A., Moiseev A. V., 2007, *MNRAS*, 381, L26  
 Massey P., Holmes S., 2002, *ApJ*, 580, L35  
 Mazzali P. A., McFadyen A. I., Woosley S. E., Pian E., Tanaka M., 2014, *MNRAS*, 443, 67  
 Moore B., Ghigna S., Governato F., Lake G., Quinn T., Stadel J., Tozzi P., 1999, *ApJ*, 524, L19  
 Oey M. S., 1996, *ApJ*, 467, 666  
 Oh S.-H., de Blok W. J. G., Brinks E., Walter F., Kennicutt, R. C., Jr. 2011a, *AJ*, 141, 193  
 Oh S.-H., Brook C., Governato F., Brinks E., Mayer L., de Blok W. J. G., Brooks A., Walter F., 2011b, *AJ*, 142, 24

- Pakmor R., Marinacci F., Springel V., 2014, *ApJ*, 783, L20  
Perley R. A., Butler B. J., 2013, *ApJS*, 204, 19  
Rau U., Cornwell T. J., 2011, *A&A*, 532, A71  
Rieger F. M., de Oña-Wilhelmi E., Aharonian F. A., 2013, *Frontiers Phys.*, 8, 714  
Salem M., Bryan G. L., 2014, *MNRAS*, 437, 3312  
Scannapieco C., 2013, *Astron. Nachr.*, 334, 499  
Siejkowski H., Otmianowska-Mazur K., Soida M., Bomans D. J., Hanasz M., 2014, *A&A*, 562, A136  
Silverman J. M., Filippenko A. V., 2008, *ApJ*, 678, L17  
Strickland D. K., Heckman T. M., 2009, *ApJ*, 697, 2030  
Thurrow J. C., Wilcots E. M., 2005, *AJ*, 129, 745  
Tremonti C. A. et al., 2004, *ApJ*, 613, 898  
Tribble P. C., 1993, *MNRAS*, 261, 57  
Wilcots E. M., Miller B. W., 1998, *AJ*, 116, 2363  
Yang H., Skillman E. D., 1993, *AJ*, 106, 1448

This paper has been typeset from a  $\text{\TeX/L\AA\TeX}$ file prepared by the author.